

Diluted magnetic semiconductor properties in $\text{Zn}_{1-x}\text{Cu}_x\text{O}$ nanoparticles synthesized by sol gel route

R. Elilarassi · P. Sambasiva Rao · G. Chandrasekaran

Received: 1 February 2010 / Accepted: 7 September 2010 / Published online: 21 September 2010
© Springer Science+Business Media, LLC 2010

Abstract Nanoparticles of ZnO:Cu Diluted Magnetic Semiconductor (DMS) are prepared using sol gel method. The structural, optical and EPR properties of them are investigated. The XRD patterns of them show the formation of polycrystalline and hexagonal wurtzite structure without any secondary phase formation. The average size of particles ranges from 14 to 19 nm. In the optical absorption study of the samples, a red shift of optical band edge and a narrowing of the optical band gap are observed when Cu concentration is increased. The PL measurements illustrate 392 nm UV radiation of the near band-edge emissions of ZnO, blue emission at 450 nm and orange emission at 628 nm. The cause of decrease in intensity of these emission lines is the sincerely enhanced non-radiative transitions when Cu is doped in ZnO. EPR measurements provide substantial evidence for the presence of defect states and enhancement of exchange interaction.

Keywords Sol-gel synthesis · DMS- Zinc-copper oxide · Nanomaterials

1 Introduction

Nanoparticles of wide band semiconductors like ZnO, TiO_2 , SnO_2 , In_2O_3 doped with transition metals have

immense and everlasting interest as they transform into technologically interesting photonic and spintronic materials. Transition element doping in these oxide semiconductors has been extensively investigated for the past few decades. Nanomaterials of them are multifunctional in nature as they exhibit coexistence of many novel magnetic, electrical and optical properties. One of the members of oxide semiconductors, ZnO is a semiconductor with a wide band gap and high exciton binding energy at room temperature. It is a promising candidate for electronics, photonics and optical device applications [1–5] such as laser diodes (LDs), optoelectronics, and sensors. Theoretical calculations have predicted room temperature ferromagnetism in ZnO doped with transition metals like Ni, Mn, Co, Cu, Cr, V and Fe. Specifically, Copper doped zinc oxide nanocrystals both in the form of thin films and powders have been reported in the literature [6–10]. For Cu ions distinctly assigned which of Cu ions is monovalent (Cu^+) presenting luminescence emission and which is divalent (Cu^{2+}) exhibiting paramagnetic effect, it is of interest to investigate its optical emission property adjunct with magnetic phase in a detail manner.

In the present study, we have synthesized nano particles of $\text{Zn}_{1-x}\text{Cu}_x\text{O}$ by a more promising sol gel route. The changes in their structural and optical and magnetic properties are accounted for by the Cu substitution in ZnO.

2 Experimental

Nanocrystalline $\text{Zn}_{1-x}\text{Cu}_x\text{O}$ ($x = 0.0, 0.02, 0.04, 0.06, 0.08$) powder samples are synthesized by a simple and wet chemical sol gel auto-combustion method using glycine as the combustion agent. Glycine is preferred ($\text{NH}_2\text{CH}_2\text{COOH}$) for fueling the combustion reaction since its

R. Elilarassi · G. Chandrasekaran (✉)
Department of Physics, Magnetism and Magnetic Materials
Laboratory, School of Physical, Chemical and Applied Sciences,
Pondicherry University, Puducherry 605 014, India
e-mail: chandra.phy@pondiuni.edu.in

P. Sambasiva Rao
Department of Chemistry, School of Physical, Chemical
and Applied Sciences, Pondicherry University, Puducherry
605 014, India

combustion enthalpy (-3.24 kcal/g) is more negative when compared with urea (-2.98 kcal/g) or citric acid (-2.76 kcal/g) and it is the most inexpensive [9]. Its chemical formula ($\text{NH}_2\text{CH}_2\text{COOH}$) has a carboxylic acid group at one end and amino group at the other end. Such donor atoms as N and O in amino and carboxylic groups, respectively, in glycine play the complexing role for a number of metal ions [11–13]. Thus auto combustion reaction allows homogenous mixing of the chemicals at atomic level and yields successfully the nanoparticles of the proposed product. In the present synthesis of $\text{Zn}_{1-x}\text{Cu}_x\text{O}$ ($x = 0.0, 0.02, 0.04, 0.06, 0.08$), $\text{Zn}(\text{NO}_3)_2 \cdot 6\text{H}_2\text{O}$, $\text{Cu}(\text{NO}_3)_2 \cdot 6\text{H}_2\text{O}$ and glycine ($\text{C}_2\text{H}_5\text{NO}_2$) are dissolved in deionized water in a large beaker to obtain a 100 ml aqueous solution. The metal ion and glycine molar ratio is maintained as 1:1. The reactants are procured from HIMEDIA Laboratory Ltd, Mumbai, India. The aqueous solution so obtained is then stirred for about 1 h in order to mix the solution uniformly. The temperature of uniformly mixed precursor solution is raised to 100°C to evaporate the excess free water in it. Subsequent stage of heating of precursor to 130°C results in repeated cycles of swelling and foaming accompanied with a strong self-propagating combustion reaction. Finally, a reticular substance obtained is ground well in an agate mortar for an hour to get powder of our interest.

The structure and phase purity of the powder samples are examined by X-Ray powder Diffraction analysis (XRD) with (PAnalytical Model: X'Pert PRO). Scanning Electron Microscope (SEM) (HITACHI Model: S-3400 N) is used to observe the microstructure of the resulting powders. A confirmation of purity of the samples is done by Energy Dispersive X Ray analysis EDX (Thermo S-3400 N) technique. FTIR spectral study is performed using SHIMADSU in the range from 400 to $1,000\text{ cm}^{-1}$. The optical absorption spectrum is recorded at room temperature using UV–Visible spectrophotometer (Model: CARY 5000) in the wavelength range from 300 to 800 nm . Room temperature Photoluminescence (PL) studies are carried out using a Spectrofluorimeter (Fluorolog-3). EPR measurements are carried out using EPR spectrograph (Jeol-100, X-Band).

3 Results and discussion

3.1 Structural study

The interpretation of structural changes can be done using the XRD patterns of $\text{Zn}_{1-x}\text{Cu}_x\text{O}$ nanoparticles which are shown in Fig. 1 for all concentrations. The observed patterns of the samples possess well resolved set of peaks as a result of single phase polycrystals in them. The XRD

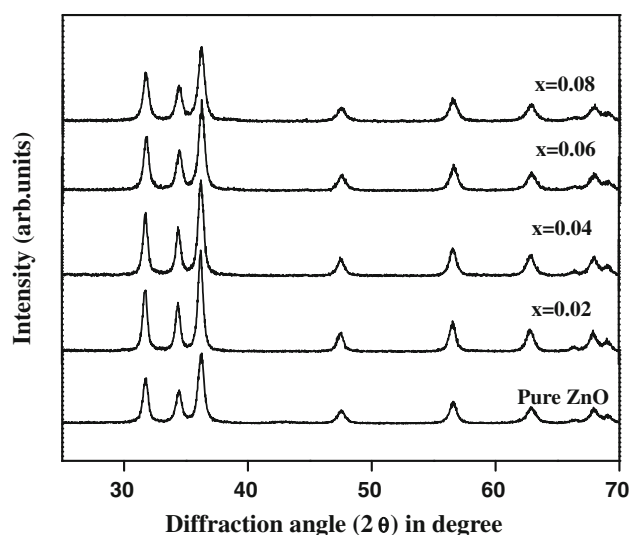


Fig. 1 X-ray diffraction patterns of $\text{Zn}_{1-x}\text{Cu}_x\text{O}$ nanoparticles

patterns of samples show a good matching with XRD standard data file i.e., JCPDS file no. 21-1486, a standard hexagonal wurtzite structure. The broadened bases of XRD peaks show that the particles have grown in nanosize. Estimation of mean particle size of the particles constituting the powder samples is done using the data of FWHM of peaks and the angle of diffraction in Scherrer's formula [14]. The observed values of particle size are given in Table 1. The size of particles ranges from 19 to 14 nm indicating a shallow decrease when diluted with Cu. The structural parameters a , c and spacing between planes d_{100} and d_{002} of the hexagonal lattice of the $\text{ZnO}:\text{Cu}$ nanoparticles are plotted with respect to concentration as shown in Fig. 2a and b respectively. It is clearly understood that Cu doping has some effect on the lattice parameters of ZnO . The decreasing trend in lattice parameters may be attributed to the difference in ionic radii of Zn^{2+} (0.074 nm) and Cu^{2+} (0.073 nm) ions [15]. Any increasing trend may be due to the presence of Cu^+ (0.077 nm) in $\text{ZnO}:\text{Cu}$ nanoparticles.

The SEM micrographs shown in Fig. 3 depict the topographical features of powdered $\text{ZnO}:\text{Cu}$ samples. A close scrutiny of the micrographic images uncovers the presence of a set of white patches and black portions surrounded with the foggy regions. The white patches signify

Table 1 Particle size of $\text{Zn}_{1-x}\text{Cu}_x\text{O}$ samples

| Sample | Particle size (nm) |
|--|--------------------|
| $\text{Zn}_{1.0}\text{Cu}_{0.0}\text{O}$ | 18.5 ± 0.8 |
| $\text{Zn}_{0.98}\text{Cu}_{0.02}\text{O}$ | 19.5 ± 0.6 |
| $\text{Zn}_{0.96}\text{Cu}_{0.04}\text{O}$ | 17.7 ± 0.5 |
| $\text{Zn}_{0.94}\text{Cu}_{0.06}\text{O}$ | 15.6 ± 0.4 |
| $\text{Zn}_{0.92}\text{Cu}_{0.08}\text{O}$ | 14.7 ± 0.4 |

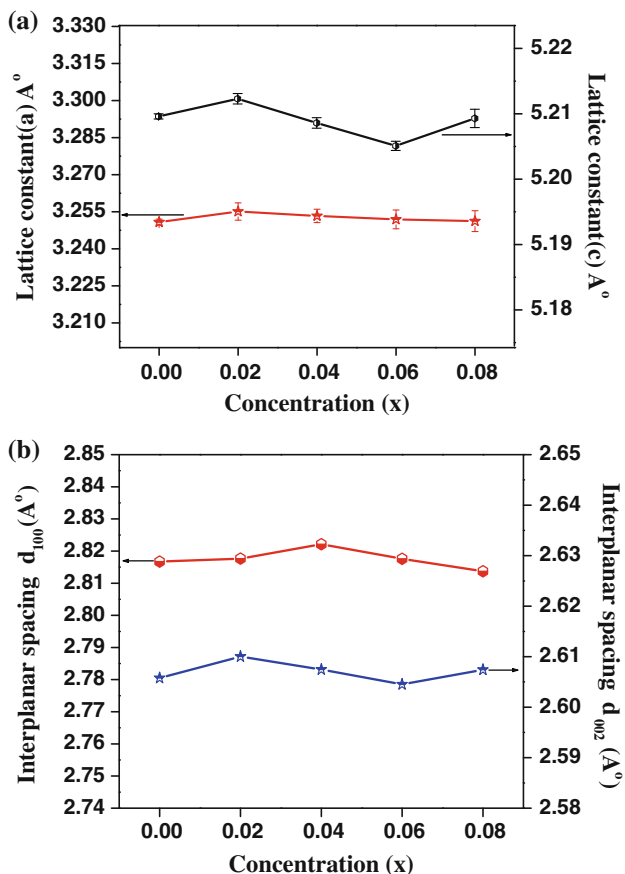


Fig. 2 a Lattice parameters of Zn_{1-x}Cu_xO nanoparticles. b Interplanar spacing of Zn_{1-x}Cu_xO nanoparticles

the clusters of ZnO:Cu nanocrystals. The black portions are the gaps created due to liberated gases during the reactions. The foggy regions are the aggregation of crystals in a bed of liquid water. It is also possible to notice that Cu doping plays an effective and substantial role on the size of the aggregation ZnO:Cu crystallites. It is observed from the micrographs that the aggregates grow larger with Cu. It is explained that the smaller crystallites, as reported in XRD study, aggregate faster to form bigger sizes of grain when Cu content rises. The particle growth is constrained whereas aggregation is speeded up.

The EDAX of ZnO:Cu nanoparticles are done for knowing the purity and presence of Cu in their composition. The observed EDAX patterns for a representative case of Zn_{0.92}Cu_{0.08}O is shown in Fig. 4. It is noticed from Fig. 4 that the samples prepared contain only Zn, Cu and O. The Cu ions are present in two compounds with oxygen i.e., CuO and Cu₂O. It clearly indicates the existence of Cu²⁺ and Cu⁺ in the ZnO:Cu nanoparticles after substituted with Cu. Thus the nanocrystallites are free from any impurity. The ratio of amount of the elements in the Zn_{0.2}Cu_{0.8}O nanoparticles complies with the quantity taken for their preparation.

3.2 FTIR study

FTIR transmittance spectra of the Zn_{1-x}Cu_xO samples are employed to study the formation of Zn–O, Cu–O bonds and vacancy sites. The FTIR spectra of Zn_{1-x}Cu_xO nanocrystallites are shown in Fig. 5. The frequency data for some important bands which show the persistent and meaningful trends are given in Table 2. The bands located near 495 cm⁻¹ correspond to stretching modes of Zn–O/Cu–O in tetrahedral coordination [16, 17]. The bands which appear between 447 and 466 cm⁻¹ [18] after substitution of Cu in ZnO would correspond to a comparatively longer Cu⁺–O bond in tetrahedral site. The i.r bands on 648 and 750 cm⁻¹ correspond to the defect states in the structure [19]. The changes in wave number of the last two bands may be attributed to the expansion and contraction of defect sites.

3.3 Optical absorption study

The optical absorption of the nanoparticles of Zn_{1-x}Cu_xO is studied using the observed UV–visible spectra and the spectra taken are shown in Fig. 6. It is seen from Fig. 6 that the band edge appearing around 380 nm shows a red shift with the enhancement of Cu content. The observed red shift in the band edge may be due to a role played by Cu on the charge transfer transitions as it would interpose a shallow number of energy levels under air band which is the famous Burstein–Moss effect [20–22]. It is an evidence for the incorporation of Cu ions into ZnO lattice. The estimation of optical absorption coefficient (α) of ZnO:Cu is carried out using the relation [20]

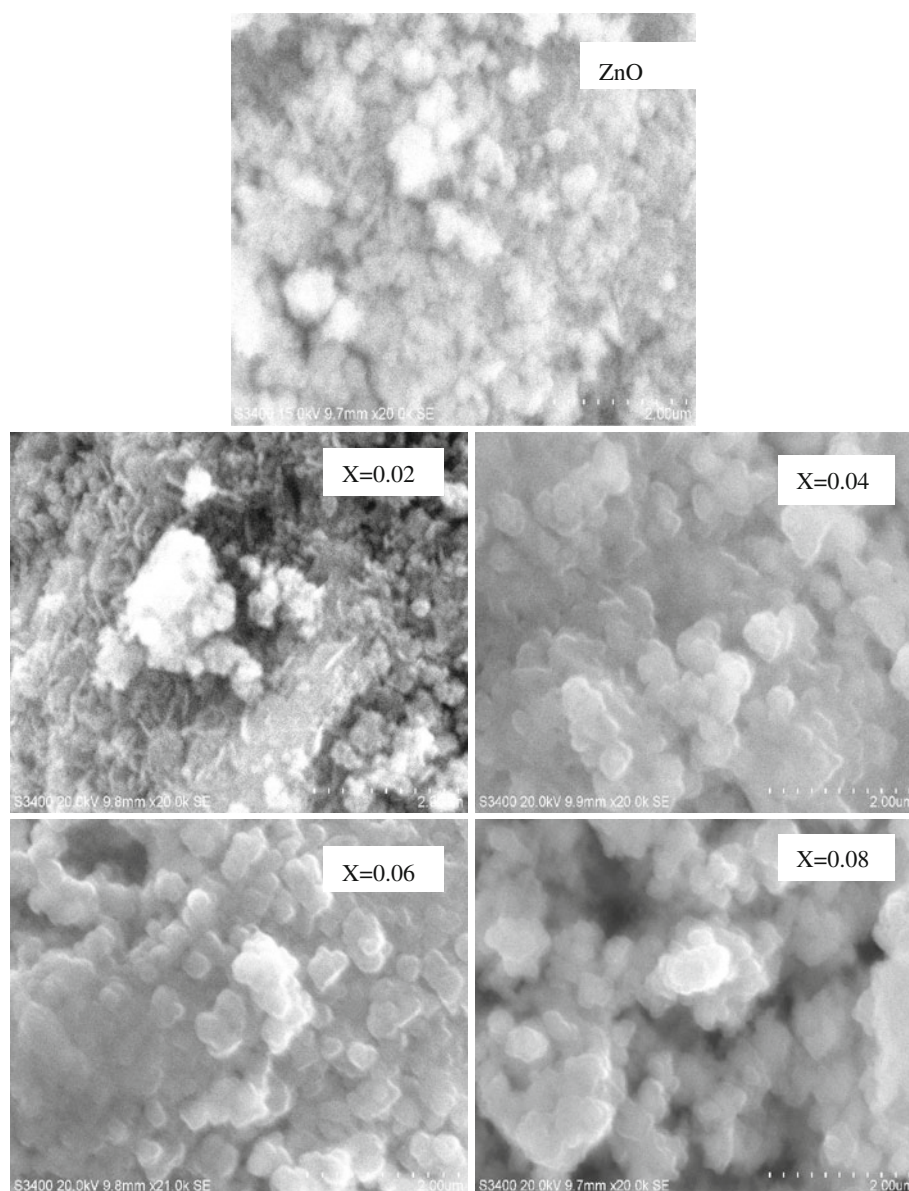
$$T = A \exp(-\alpha d) \tag{1}$$

where T is the transmittance of nanoparticles obtained by reciprocating the absorption at any frequency observed from Fig. 6 and d is the average size of particle. The constant A is approximately unity, as the reflectivity is negligible and insignificant near the absorption edge. The optical band gaps of the ZnO:Cu nanoparticles are determined by fitting to the Tauc model [23] and the Davis and Mott model [24] in the high absorbance region:

$$(\alpha h\nu)^2 = D(h\nu - E_g) \tag{2}$$

where $h\nu$ is the photon energy, E_g is the optical band gap, and D is a constant. For a direct transition, square form of $(\alpha h\nu)$ is chosen since it gives the best fit linear curve in the band-edge region. The relationship between $(\alpha h\nu)^2$ and $h\nu$ is brought out by plotting a graph as shown in Fig. 7a. The values of E_g are estimated by extrapolating the vertical line portion to cut the photon energy axis in the Fig. 7a. The values of band gap so obtained are plotted against concentration of Cu in ZnO and it is shown in Fig. 7b. It

Fig. 3 SEM micrographs of $Zn_{1-x}Cu_xO$ nanoparticles



is found that the band gap decreases with increasing copper content. It is reasonable to expect a decrease in the band gap of the nanoparticles with increasing Cu concentrations as the band gap of CuO (1.4 eV) is less than that of ZnO (3.3 eV). Bylsma et al. [25] has explained theoretically that the exchange interactions of magnetic ions are responsible for the change in band gap with varying dopant concentration using second-order perturbation theory. Thus the short-ranged exchange interactions developed by Cu ions are more pronounced in the case of nanocrystalites. The observation of a systematic decrease of the band gap in ZnO nanocrystals as a direct function of the Cu content is explained on the basis of the encroachment of shallow energy levels below the air band of ZnO. An expected energy band picture suitably explaining band gap narrowing is depicted in a diagram

[26] as shown in Fig. 8. The diagram can lend support for the absorption bands in the spectra of the $Zn_{1-x}Cu_xO$ nanoparticles in correlation with the transitions of tetrahedral coordination of Cu^{2+} and Cu^+ ions which are assigned as the spin-orbit split ${}^3T_1(F) \rightarrow {}^3T_1(P)$ ligand field transitions [27]. In order to confirm the mechanism of formation of bands, a theoretical calculation of band gap needs to be done and a comparison of the calculated and empirical values of band gap render a support for the explanation. The band gap of the nanoparticles is theoretically calculated using the formula proposed by Kayanuma [28] and Kim et al. [29].

$$E_{(\text{gap, nanocrystal})} = E_{(\text{gap, bulk})} - 0.248E_{Ry}^* + \frac{\pi^2 \hbar^2}{2R^2} \left(\frac{1}{m_e^*} + \frac{1}{m_h^*} \right) \quad (3)$$

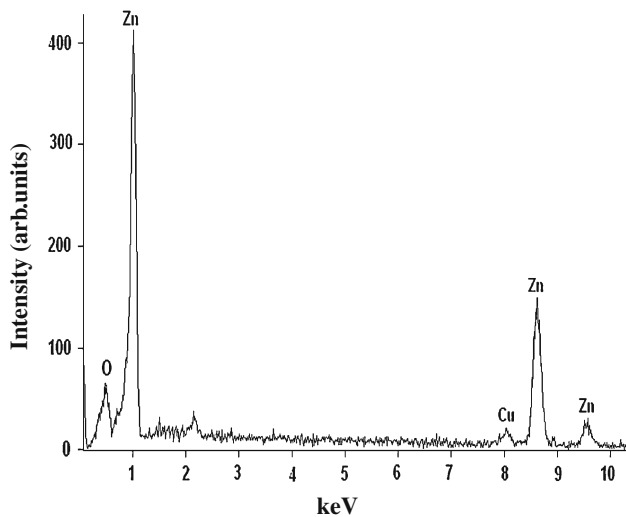


Fig. 4 A representative EDAX pattern of Zn_{0.92}Cu_{0.08}O nanoparticles

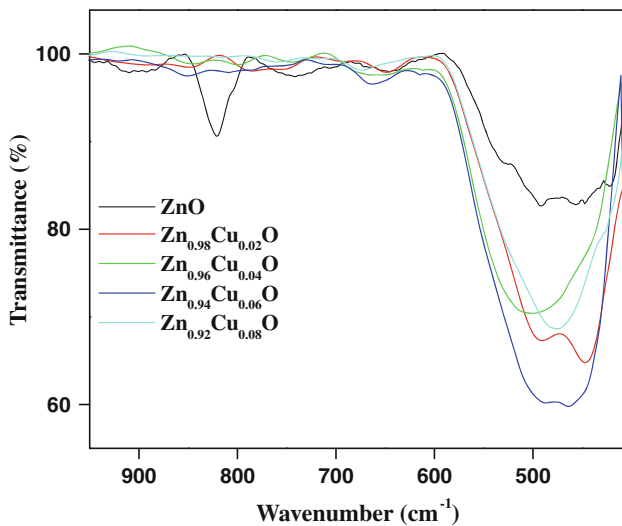


Fig. 5 FTIR spectra of copper doped ZnO:Cu nanoparticles

Table 2 Frequencies of vibration band of Zn_{1-x}Cu_xO nanoparticles

| Concentration (x) | Wave numbers (cm ⁻¹) | | | |
|-------------------|----------------------------------|-----|-----|-----|
| 0.00 | – | 495 | 648 | 750 |
| 0.02 | 447 | 490 | 653 | 756 |
| 0.04 | 458 | 500 | 654 | 744 |
| 0.06 | 463 | 493 | 662 | 761 |
| 0.08 | 466 | 493 | 655 | 759 |

The bulk band gap $E_{(\text{gap, bulk})}$ is taken as 3.2 eV; the bulk exciton binding energy E_{Ry}^* is taken as 60 meV [30]; the electron and hole effective masses are taken as $m_e^* = 0.24m_o$ [31] and $m_h^* = 2.31m_o$ [32] respectively; ‘h’ is

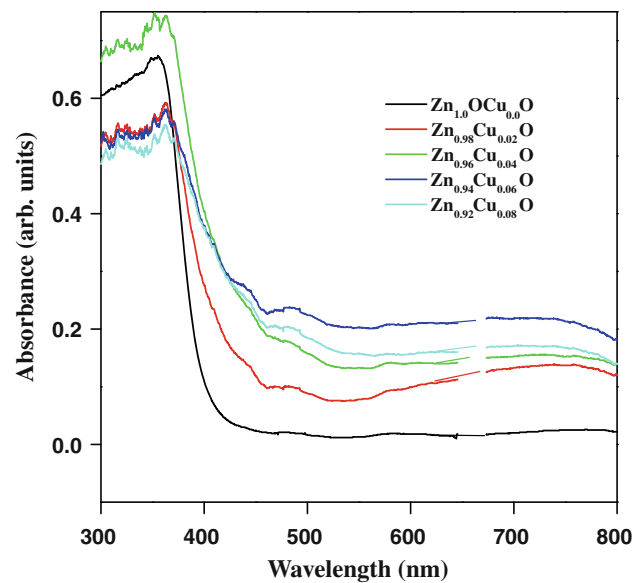


Fig. 6 UV-Visible absorbance spectra of Cu-doped ZnO nanoparticles

Planck’s constant and ‘R’ is the mean radius of ZnO nanograins. It is noticed from Fig. 8 that the values of the theoretical and the experimental band gaps show a good agreeable trend.

3.4 Photoluminescence study

Room temperature photoluminescence spectra of the Zn_{1-x}Cu_xO nanoparticles are recorded in the range from 360 to 700 nm using a spectrofluorimeter having Xe laser source of excitation wavelength 350 nm and shown in Fig. 9a. PL spectra of ZnO:Cu nanoparticles consist of a strong ultraviolet-emission band at 392 nm (3.16 eV), strong blue and orange emission peaks centered around 450 nm (2.75 eV) and 628 nm (1.97 eV) respectively. The UV emission peak at 392 nm can be attributed to the radiative recombination of bound excitons corresponding to band-edge emission of ZnO [33–35]. The intense blue emission peak at 450 nm can be attributed to the intrinsic defects such as shallow or deep donor level due to oxygen vacancies or interstitial zinc located 0.5 eV below the conduction band in ZnO [36]. The strong bands get weakened when Cu content is enhanced in ZnO matrix as shown in Fig. 9b. The weak blue-green emission bands observed near 468, 481 and 491 nm in ZnO nanoparticles diminish very much upon copper doping. The quenching of intensity of strong emissions by Cu doping may be assigned to the reduction in the probability of recombination of electrons and holes in d bands. The many fold intensity decrease of excitonic weak blue and green emissions may also be due to the suppression of charge transfer

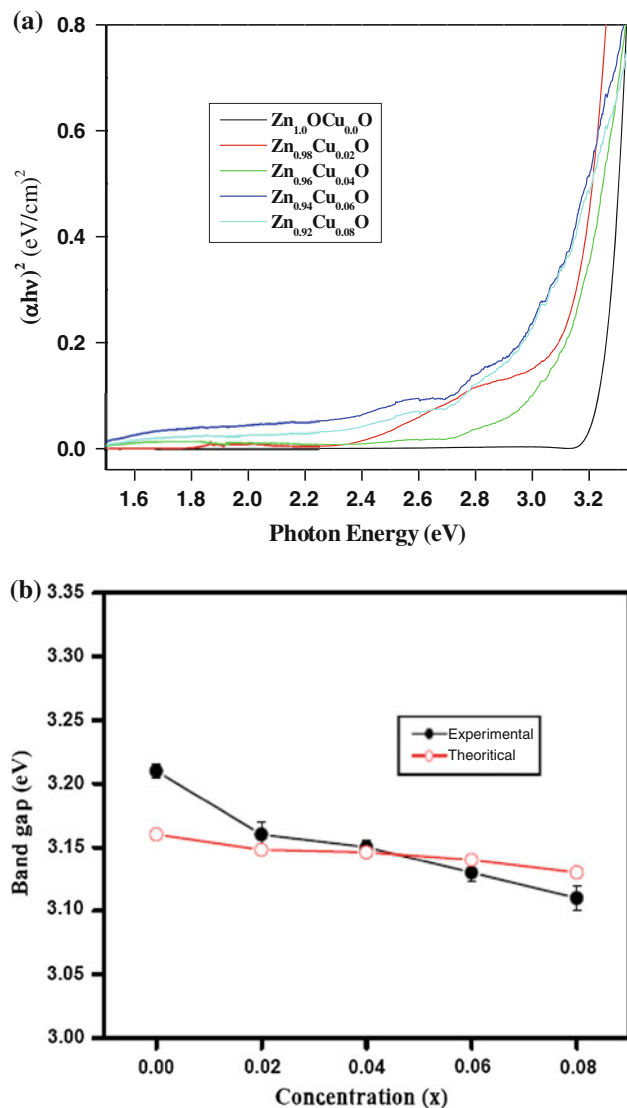


Fig. 7 **a** $(\alpha hv)^2$ versus photon energy (hv) Cu-doped ZnO nanoparticles. **b** Experimental and theoretical band gaps versus doping concentration of Cu

transitions by copper. The magnetically active Cu ions would create spin–orbit and exchange interactions i.e., the sp-d exchange interactions between the band electrons and the localized d-electrons of the Cu²⁺ ions [37] which are also responsible for the blossoming of magnetic phase. The coupling of magnetic interactions with optical modes by relaxation processes develops the hindrances to the recombination process or transfer of charge carriers.

3.5 EPR study

The roles of exchange interaction and the defect centers in diluted magnetic semiconductors are understood from EPR spectra [38–41]. The EPR spectra taken for ZnO:Cu

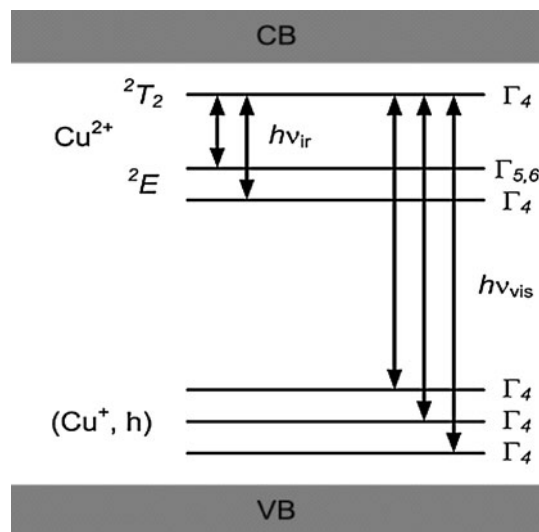


Fig. 8 Energy states of Copper in ZnO. Ref. [25]

nanoparticles are shown in Fig. 10a and b. The Fig. 10a is a spectrum of ZnO nanoparticles showing a weak EPR signal in the range of field of 335 ± 15 mT. It is explained to be due to the defect centers in ZnO i.e., either Zn²⁺ vacancy or electronic jumps near the O²⁻ ions [42]. The spectra for Cu deposited ZnO nanoparticles in Fig. 10b show that they have invariably the strong and broad peaks centered at 100 in a range of field of 100 ± 100 mT. The observed values of g, line width and relaxation time are given in Table 3. The EPR parameters are able to clearly bring out two entirely different transitions in ZnO:Cu nanoparticles. The strong and broad signals appearing after the substitution of Cu ions are undoubtedly indicative of the interactions developed around the Cu ions. The presence of Cu⁺ and Cu²⁺ is confirmed from PL and exchange interaction respectively. Thus Cu⁺ ions create dipolar interaction and Cu²⁺ ions cause an environment for exchange interactions. Hence a broad signal is caused by the coexistence of different valence states of Cu ions. The spin lattice relaxation time reduces in the deposited ones to 1/10th of its value in pure ZnO nanoparticles and shows a gradual decrease with increase of Cu concentration. The XRD study of the present samples showed a decrease of particle size (refer Table 1). The spin lattice relaxation time reduction is attributed to the decrease in the particle size. Thus EPR study on ZnO:Cu nanoparticles establishes a fact that a shortening of the interval of relaxation processes is caused by the densification of magnetically active energy levels of Cu in the forbidden region of ZnO when Cu is increased. The energy levels of Cu are already shown in Fig. 8 and charge carriers occupying them are sensitive to localized fields. Ultimately probability of failure in the recombination of holes and electrons is enhanced i.e., non

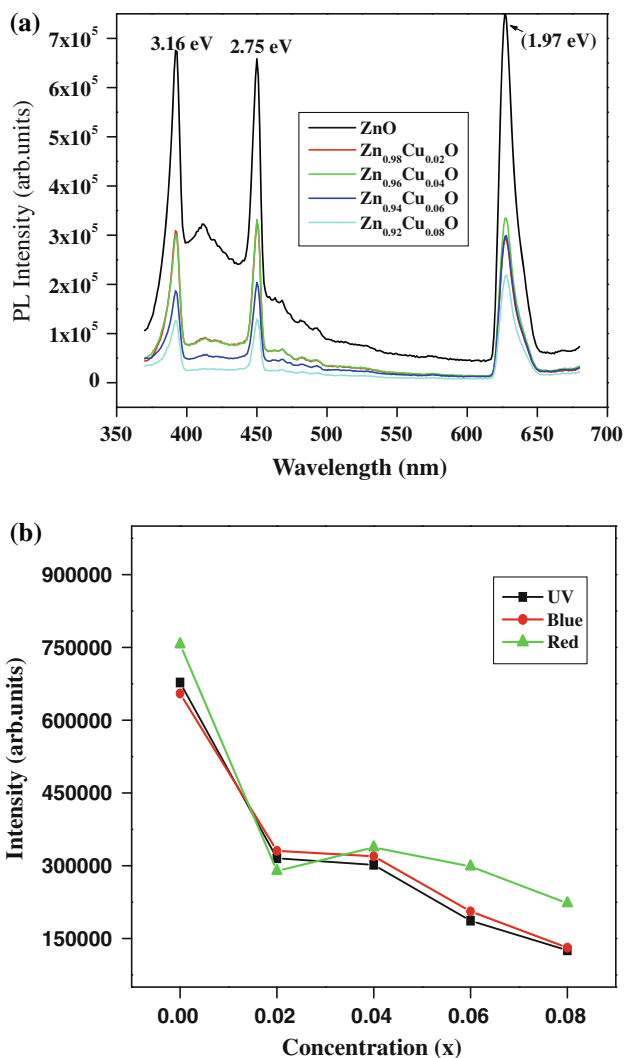


Fig. 9 **a** PL spectra of Zn_{1-x}Cu_xO nanoparticles with an excitation wavelength of 350 nm. **b** PL emission intensity versus doping concentration of Cu-doped ZnO nanoparticles

radiative excitonic transitions from defect states become more prevalent. The shortening of spin lattice interaction due to Cu indicates that the enhanced magnetic exchange interaction suppresses radiative optical transitions. This is a quantum behaviour observed when ZnO nanoparticles are deposited with Cu in a dilute quantity.

4 Conclusion

The Zn_{1-x}Cu_xO nanoparticles (x = 0.00, 0.02, 0.04, 0.06, 0.08) are successfully synthesized using sol-gel auto-combustion method, using glycine as combusting material. XRD study on ZnO:Cu reveals that Cu ions are incorporated into the wurtzite lattice sites, without any secondary phase and the possible presence of Cu⁺. FTIR spectral

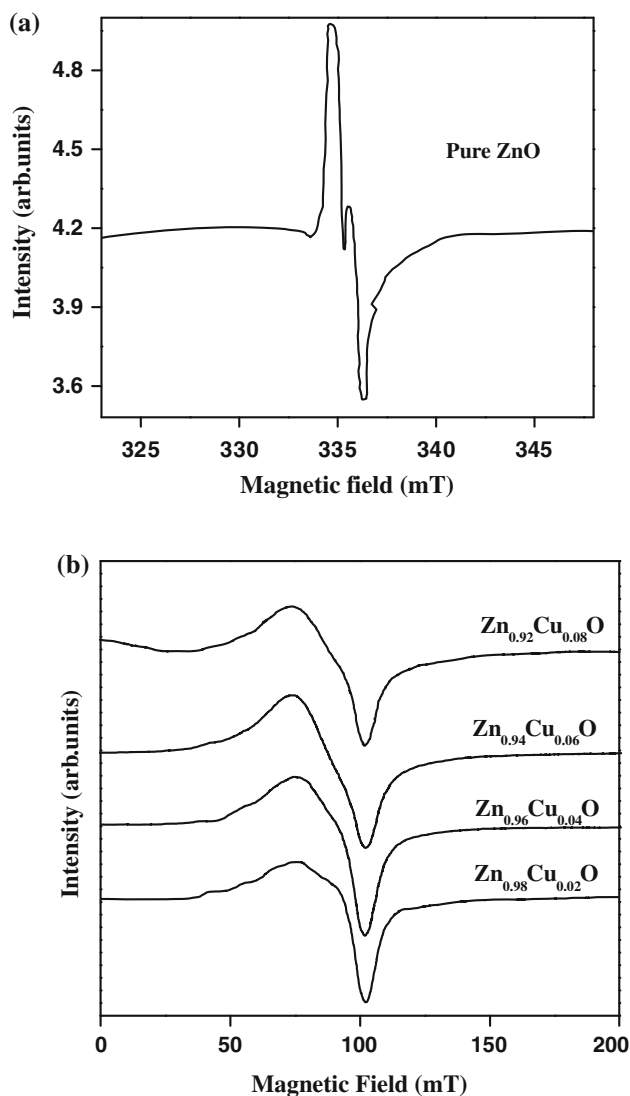


Fig. 10 **a** EPR spectrum of ZnO nanoparticles. **b** EPR spectra of ZnO:Cu nanoparticles

Table 3 EPR parameters of Zn_{1-x}Cu_xO nanoparticles

| Concentration (x) | g-value | Line width (mT) | Spin-spin relaxation time (10 ⁻⁹ s) |
|-------------------|-----------------|-----------------|--|
| 0.00 | 2.0201 ± 0.0013 | 1.406 | 2.310 |
| 0.02 | 2.3084 ± 0.0005 | 24.847 | 0.1145 |
| 0.04 | 2.3200 ± 0.0004 | 26.277 | 0.1076 |
| 0.06 | 2.3210 ± 0.0012 | 27.736 | 0.1019 |
| 0.08 | 2.3232 ± 0.0010 | 28.466 | 0.0992 |

study confirms the formation of Zn_{1-x}Cu_xO nanoparticles with Zn and Cu ions in tetrahedral coordination and also existence of the vacancy sites. A red-shift in the band gap with the increasing copper content is an evidence for diffusing in of diluted magnetic phase in ZnO matrix. The

magnetic interactions quench strong and weak emission bands in PL. The particle size dependence of spin lattice relaxation time in EPR study beautifully portrays the suppressing of the recombination process in ZnO:Cu nanoparticles as transfer of the charge carriers are hindered by the magnetic interactions created in the neighbourhoods of Cu ions.

Acknowledgments Authors are thankful to DST- FIST New Delhi, India for funding XRD in Department of Physics, Faculties of Central Instrumentation Facility for their help in SEM, EDAX, FTIR and PL characterizations and Department of Chemistry, Pondicherry University for permission to use EPR and UV–Visible spectrographs.

References

- Huang M, Mao S, Feick H, Yan H, Wu Y, Kind H, Weber E, Russo R, Yang P (2001) *Science* 292:1897
- Das Sarma S (2001) *Am Sci* 89:516
- Law M, Greene LE, Johnson JC, Saykally R, Yang P (2005) *Nat Mater* 4:455
- Major WS, Banerjee A, Chopra KL, Nagpal KC (1986) *Thin Solid Films* 143:19
- Aktaruzzaman AF, Sharma GL, Malhotra LK (1991) *Thin Solid Films* 198:67
- Borghain K, Mahamuni S (1998) *Semicond Sci Technol* 13:1154
- Bhargava RN, Chhabra V, Som T, Ekimov A, Taskar N (2002) *Phys Status Solidi B* 229:897
- Ranjani Viswanatha S, Chakraborty S, Basu S, Sarma DD (2006) *J Phys Chem B* 110:22310
- Risbud AS, Spaldin NA, Chen ZQ, Stemmer S, Seshadri Ram (2003) *Phys Rev B* 68:205202
- Fernandes DM, Silva R, Winkler Hechenleitner AA, Radovanovic E, Custódio Melo MA, Gómez Pineda EA (2009) *Mater Chem Phys* 115:110
- Hwang Chyi-Ching, Wu Tsung-Yung (2004) *J Mater Sci* 39:6111
- Purohit RD, Sharma BP, Pillai KT, Tyagi AK (2001) *Mater Res Bull* 36:2711
- Deka S, Joy PA (2005) *Solid State Commun* 134:665
- Cullity BD (1978) *Elements of X-Ray diffractions*. Addison-Wesley, Reading
- Shannon RD (1976) *Acta Cryst* A32:751
- Waldron RD (1955) *Phys Rev* 99(6):1727
- Cozzoli PD, Curri ML, Agostiano A, Leo G, Lomascolo M (2003) *J Phys Chem B* 107:4756
- Xi Y, Sudakar C, Kharel P, Lawes G (2007) *J Phys Condens Matter* 19:026212
- Conga CJ, Honga JH, Zhanga KL (2009) *Mat Chem Phys* 113:435
- Miyata T, Suzuki S, Ishii M, Minami T (2002) *Thin Solid Films* 411:76
- Roth AP, Webb JB, Williams DF (1981) *Solid State Commun* 39:1269
- Jeon KA, Kim JH, Shim WY, Lee WY, Jung MH, Lee SY (2006) *J Cryst Growth* 287:66
- Tauc J (1974) *Amorphous and liquid semiconductors*. Plenum, London
- David EA, Mott NF (1970) *Philos Mag* 22:903
- Bylsma RB, Becker WM, Kossut J, Debska U, Yoder-Short D (1986) *Phys Rev B* 33:8207
- Dahan P, Fleurovy V, Thuriann P, Heitz R, Hoffmannz A, Broserz I (1998) *J Phys Condens Matter* 10:2007
- Weaklim HA (1962) *J Chem Phys* 36:2117
- Kayanuma Y (1988) *Phys Rev B* 38:9797
- Kim KK, Koguchi N, Ok YW, Seong TY, Park SJ (2004) *Appl Phys Lett* 84:3810
- Pearton SJ, Norton DP, Ip K, Heo YW, Steiner T (2005) *Prog Mater Sci* 50:293
- Beni G, Rice TM (1978) *Phys Rev B* 18:768
- Fan WJ, Xia JB, Agus PA, Tan ST, Yu SF, Sun XW (2006) *J Appl Phys* 99:013702
- Monticone S, Tufeu R, Kanaev AV (1998) *J Phys Chem B* 102:2854
- Nikitenko VA, Malov MM, Pasko PG, Chernuj VD (1974) *J Appl Spectrosc* 21:835
- Liu DH, Liao L, Li JC, Guo HX, Fu Q (2005) *Mater Sci Eng B* 121:77
- Baek S, Song J, Lim S (2007) *Physica B* 399:101
- Yang P, Lieber CM (2002) *Nature* 419:553
- Moribe Shinya, Ikoma Tadaaki, Akiyama Kimio, Zhang Qiwu, Saito Fumio, Tero-Kubota Shozo (2007) *Chem Phys Lett* 436:373
- Nikitenko VA (1994) *J Appl Spectrosc* 56:783
- Vlasenko LeonidS (2009) *Physica B* 404:4774
- Liu WilliamK, Whitaker KellyM, Smith AlyssaL, Kittilstved KevinR, Robinson BruceH, Gamelin DanielR (2007) *Phys Rev Lett* 98:186804
- El Mira L, El Ghoul J, Alaya S, Ben Salem M, Barthou C, von Bardeleben HJ (2008) *Physica B* 403:1770